Mathematical Biosciences and Engineering

MBE, 19(9): 8648−8670.
DOI: 10.3934/mbe.2022401
Received: 17 April 2022
Revised: 02 June 2022
Accepted: 04 June 2022
Published: 16 June 2022

http://www.aimspress.com/journal/MBE

Research article

Optimizing thermal efficiencies of power-law fluids in double-pass concentric circular heat exchangers with sinusoidal wall fluxes

Chii-Dong Ho[1,*], Jr-Wei Tu[1], Hsuan Chang[1], Li-Pang Lin[1] and Thiam Leng Chew[2,3]

[1] Department of Chemical and Materials Engineering, Tamkang University, 151 Yingzhuan Road, Tamsui, New Taipei, Taiwan 251
[2] Department of Chemical Engineering, Faculty of Engineering, Universiti Teknologi Petronas, 32610 Seri Iskandar, Perak Darul Ridzuan, Malaysia
[3] CO2 Research Center (CO2RES), Institute of Contaminant Management Universiti Teknologi Petronas, 32610 Seri Iskandar, Perak Darul Ridzuan, Malaysia

* **Correspondence:** Email: cdho@mail.tku.edu.tw; Tel: +1886226215656 ext. 2724; Fax: +1886226209887.

Abstract: Effect of external-recycle operations on the heat-transfer efficiency, specifically for the power-law fluid flowing in double-pass concentric circular heat exchanger under sinusoidal wall fluxes, is investigated theoretically in the developed countries. Given that the fluid is heated twice on both sides of the impermeable sheet, four flow patterns proposed in recycling double-pass operations are expected to make substantial improvements in the performance of heat exchanger device in this study. Theoretical predictions point out that the heat-transfer efficiency increases with the ratio of channel thickness of double-pass concentric circular heat exchanger for all new designs under the same working dimension and the operational condition. The fluid velocity within the double-pass heat exchanger is increased by the fluids flowing through divided subchannels, which contributed to the higher convective heat-transfer efficiency. A simplified mathematical formulation was derived for double-pass concentric circular heat exchangers and would be a significant contribution to analyze heat transfer problems with sinusoidal wall fluxes at boundaries. The results deliver the optimal performance for the proposed four configurations with the use of external recycle compared to those conducted in single-pass, where an impermeable sheet is not inserted. The influences of power-law index and impermeable-sheet position on average Nusselt numbers under various flow patterns are also delineated. The distribution of dimensionless wall temperature was lower at the level of relative smaller thickness of annular channel, and the average Nusselt numbers

for four external-recycle configurations and single-pass device were more suitable for operating under same condition. The ratio of the power consumption increment to heat-transfer efficiency enhancement demonstrates the economic feasibility among various configurations of double-pass concentric circular heat exchanger. The results also show that the external-recycle configuration (say Type B in the present study) serves as an important economic advantage in designing concentric circular heat exchangers for heating power-law fluids due to the smaller volumetric flow rate in annular channel with exiting outlet temperature.

Keywords: heat-transfer efficiency; power-law fluids; sinusoidal wall fluxes; conjugated graetz problem; external recycle

1. Introduction

The studies on heat-transfer problems applied to Newtonian fluids flow in bounded conduits play an important role to design the more efficient heat-transfer module, especially for cylindrical or parallel-plate geometries. The theoretical modeling coupled with negligible axial conduction has been successfully reduced to the simple case of single-pass operations, which is known as the classical Graetz problem [1,2]. However, more flowing streams devices (say multi-stream or multiphase systems), analogous to heat exchangers, are fundamentally different due to conjugating boundary conditions at the boundaries, referred to as conjugated Graetz problems [3,4]. It was widely used in evaporators [5], condensers [6], distillation [7], and extraction [8]. And a general formalism of temperature profiles was developed [9] through the technique of orthogonal expansion [2,3]. Many industrial products such as food processing, polymeric systems, biological process, pulp and paper suspensions [10] display non-Newtonian fluid characteristics including shear-thinning or shear-thickening behavior [11,12]. Such features had been studied on sedimentation [13] and flows over various shapes [14] including a heated cylinder [15], an inclined square [16], and C-shaped cavity [17]. Moreover, it was commonly used in the single-screw extruder for polymer processing [18] and for multiphase fluids [19]. Those non-Newtonian fluids may be treated as the laminar flow conditions with negligible viscoelastic effects in the applicable range of shear rate [20] to pursue analytical solutions. This is analogous to dealing with Newtonian fluids and to investigating the influence of shear-thinning or shear-thickening on the convective heat transfer. The aspects of non-Newtonian fluids have miscellaneous and complicated manners including both viscosity and shear rate changing [21], which were used widely in various applications [22]. The non-Newtonian fluid was studied using the power-law model [23] due to its simplicity [24]. A large body of literature has shown the practicability and feasibility of the power-law model for non-Newtonian flows by using LBM (Lattice Boltzmann Method); it was simulated by Aharonov and Rothman [25] for the first time. Delouei et al. [26] used the immersed boundary- LBM to investigate non-Newtonian fluid flow over a heated cylinder.

Utilizing a suspension of MEPCMs as a coolant [27] to explore the effect of MEPCM-suspensions [28] proves improve the heat transfer of a microchannel heatsink [29]. Dispersing the Nano-Encapsulated Phase Change Materials (NEPCMs) [30,31] in a liquid leads to a higher surface of heat transfer between the liquid and nanoparticle. Metal foams of PCMs (phase change materials) and nanoparticles of NEPCMs (nano-encapsulated phase change materials) were used recently to augment the heat-transfer characteristics under several applications in thermal and energy storage

managements, such as variable heat loads [32] and non-uniform magnetic sources [33]. They consider forced convection [34] and natural convection flow [35] of NEPCMs nanoparticles in microchannels as well as under wall vibrations [36]. The effect of using NEPCM materials as water base working-fluids to enhance the heat transfer in microchannels was studied theoretically [37]. It validated the improvement of the natural [38] or mixed convection [39] of heat transfer with the presence of NEPCMs particles. A power-law fluid flowing through a laminar countercurrent-flow double-pass concentric-tube heat exchanger, which inserts an impermeable sheet in parallel with sinusoidal wall fluxes, was investigated theoretically. Furthermore, it was devoted to investigating the device performance in applying to the engineering field concerning the distributions of the conduit wall and fluid temperature under the uniform wall temperature (Dirichlet problem) [40,41], uniform heat flux (Neumann problem) [42,43], as well as the non-uniform of sinusoidal wall heat flux [44] in both periodic [45] and circumferential [46] heating systems.

The heat-transfer efficiency and temperature distributions were solved analytically through the resultant conjugated partial differential equations by the superposition technique using the Frobenius method. Comparisons proposed for four external-recycle configurations entail the advantageous effect in promoting the enhancement in convective heat-transfer coefficient within concentric circular heat exchangers. While the disadvantageous effect falls on operating double-pass devices with remixing at the entrance. The introduction of various external-recycle configurations offers an appropriate selection to outweigh the disadvantage of remixing effect and to secure the advantage of the velocity profile of shear-thinning fluid in the conventional circular-tube heat exchanger. Providing economic considerations for recycling operations through a series of comparison of flow patterns using the recycle ratio and impermeable-sheet position is the main contribution of this work. It is believed that the accessibility of such a simplified mathematical formulation achieved here for double-pass concentric circular heat exchangers is valuable and would be a significant contribution to analyze heat transfer problems with sinusoidal wall fluxes at boundaries. The same mathematical statement undoubtedly occurs in dealing with many other possible geometric designs and boundary conditions. An analytical solution of the heat transfer problem for a countercurrent flow in double-pass operations with external fluxes is given in Section 2, which was solved in a straightforward bearing by utilizing the Frobenius method. The external-recycle configurations investigated in our earlier study [47] showed that a considerable enhancement on the device performance was made by providing an economic and technical feasibility. The present design has some practical modes of recycling double-pass heat exchangers in industrial engineering processes. The purpose of the present study is to develop the suitable design strategy theoretically and classify the optimal operation conditions such as recycle ratio and volumetric flow rate, which allows, from economic standpoints, the specification setting to achieve the higher level of the heat transfer efficiency relative to the power consumption increment.

2. Flow patterns and mathematical formulations

An impermeable sheet was inserted into a circular tube of inside diameter 2R and length L to separate the conduit into two channels, which conducts a double-pass concentric circular heat exchanger with external recycle. The thickness of the inner (subchannel a) and annular tube (subchannel b) are κR and $(1-\kappa)R$, respectively. Comparing with the radius of outer circular tube R, the thickness of the impermeable barrier δ is negligible and thermal resistant ($\delta << R$). The various flow configurations with the external recycle were illustrated by the schematic view for both recycling

concurrent- and countercurrent-flow operations, as shown in Figures 1−4. It is obvious that those external-recycle designs can enhance the heat-transfer efficiency due to the enlargement in convective heat-transfer coefficient on both sides of the impermeable sheet to the power-law fluid. Moreover, various external-recycle types were compared by the Nusselt number to find the optimal device performance to consider the heat-transfer improvement and the rise in power consumption.

Type A: Equal flow rate of both channels

The fluid with volumetric flow rate V and temperature T_i is well mixed for the fluid exiting from the lumen channel with the volumetric flow rate MV and $T_{b,0}$ before entering the inner channel for the second time, as illustrated in Figure 1 of Flow pattern A in this study. A conventional pump situated at the beginning of the lumen channel to regulate the recycling volumetric flow rate. The purpose of this recycling loop was to heat the fluid flowing twice through both channels of the concentric circular heat exchanger under sinusoidal heat fluxes $q_w''(z) = q_0''[1 + sin(\beta z)]$ on the outer wall, and thus, the double-pass operation is then repeated. Various external-recycle types designed in this study are illustrated by Type A in Figure 1.

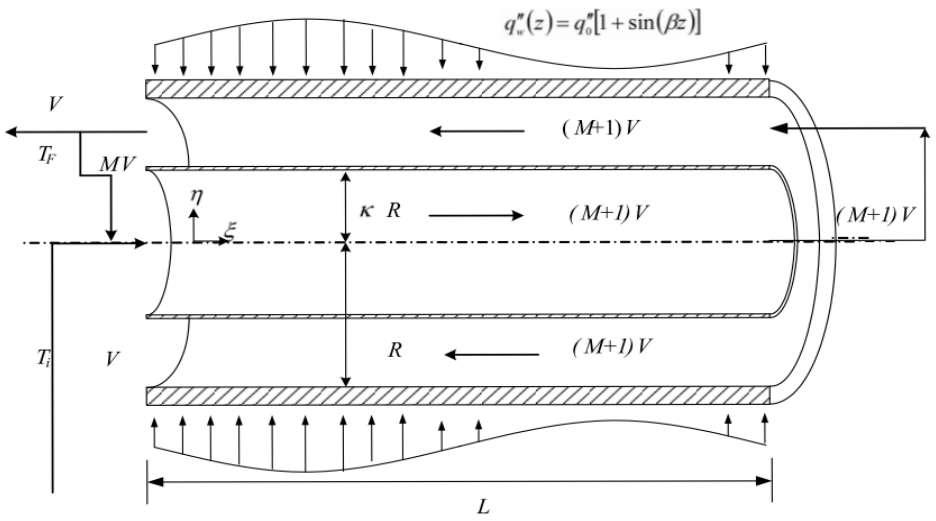

Figure 1. A schematic drawing of recycling double-pass concentric circular heat exchanger (Type A).

The problem of laminar heat transfer at steady state with negligible axial conduction, known as the Graetz problem, was studied theoretically by applying the Navier-Stokes relations to generate the hydro-dynamical equation and making energy balance with the energy-flow diagram. By following the same procedure performed in our previous work [47] and rearranging with $\xi = z/L$, one obtains the energy balance equations of fluid flowing in the inner channel and annular channel in dimensional form with specified velocities as follows:

$$\left(\frac{v_a(\eta)R^2}{\alpha GzL}\right)\frac{\partial\varphi_a(\eta,\xi)}{\partial\xi} = \frac{1}{\eta}\frac{\partial}{\partial\eta}\left(\eta\frac{\partial\varphi_a(\eta,\xi)}{\partial\eta}\right) \tag{1}$$

$$\left(\frac{v_b(\eta)R^2}{\alpha GzL}\right)\frac{\partial\varphi_b(\eta,\xi)}{\partial\xi}=\frac{1}{\eta}\frac{\partial}{\partial\eta}\left(\eta\frac{\partial\varphi_b(\eta,\xi)}{\partial\eta}\right) \tag{2}$$

The explanations of two or more contiguous streams of multi-channel problems with coupling mutual boundary conditions [48,49] becomes

$$\frac{\partial\varphi_a(0,\xi)}{\partial\eta}=0 \tag{3}$$

$$\frac{\partial\varphi_b(1,\xi)}{\partial\eta}=1+sin(B\xi) \tag{4}$$

$$\frac{\partial\varphi_a(\kappa,\xi)}{\partial\eta}=\frac{\partial\varphi_b(\kappa,\xi)}{\partial\eta} \tag{5}$$

$$\varphi_a(\kappa,\xi)=\varphi_b(\kappa,\xi) \tag{6}$$

in which

$$\eta=\frac{r}{R},\ \kappa=\frac{R_1}{R},\ \xi=\frac{z}{LGz},\ \varphi_a=\frac{k(T_a-T_i)}{q_0^{''}R},\varphi_b=\frac{k(T_b-T_i)}{q_0^{''}R},\ B=\beta GzL=2\pi Gz,\ Gz=\frac{4V}{\alpha\pi L} \tag{7}$$

For the case of our previous work [47] with $M=0$ of Type A in Figure 1. Now, the velocity distributions of Type A in subchannels *a* and *b*, say v_a and v_b, are shown as follows:

$$v_a=\left(\frac{3\omega+1}{\omega+1}\right)\frac{Q_a}{\pi(\kappa R)^2}\left[1-\left(\frac{\eta}{\kappa}\right)^{\frac{\omega+1}{\omega}}\right]=G\left[1-\left(\frac{\eta}{\kappa}\right)^{\frac{\omega+1}{\omega}}\right],\ 0\le\eta\le\kappa \tag{8}$$

$$v_b=-\frac{\left(3+\frac{1}{\omega}\right)Q_b}{\pi R^2\left[(1-\beta^2)^{1+\frac{1}{\omega}}-\kappa^{1-\frac{1}{\omega}}(\beta^2-\kappa^2)^{1+\frac{1}{\omega}}\right]}\int_\kappa^\eta\left(\beta^2\frac{1}{\eta}-\eta\right)^{\frac{1}{\omega}}d\eta=-H\int_\kappa^\eta\left(\beta^2\frac{1}{\eta}-\eta\right)^{\frac{1}{\omega}}d\eta,\ \kappa\le\eta\le\beta \tag{9}$$

$$v_b=-\frac{\left(3+\frac{1}{\omega}\right)Q_b}{\pi R^2\left[(1-\beta^2)^{1+\frac{1}{\omega}}-\kappa^{1-\frac{1}{\omega}}(\beta^2-\kappa^2)^{1+\frac{1}{\omega}}\right]}\int_\eta^1\left(\eta-\beta^2\frac{1}{\eta}\right)^{\frac{1}{\omega}}d\eta=-H\int_\eta^1\left(\eta-\beta^2\frac{1}{\eta}\right)^{\frac{1}{\omega}}d\eta,\ \beta\le\eta\le1 \tag{10}$$

where, the values of β $(v_b(\beta)=v_{b,max})$ in Eqs (9) and (10) for Type A were obtained [50] with ω and κ as parameters. The general form of dimensionless temperature distributions of the laminar double-pass concentric circular heat exchangers with sinusoidal wall fluxes can be expressed as follows [51]:

$$\varphi_a(\eta,\xi) = \theta_{0a}\xi + \theta_{1a}(\eta) + \theta_{2a}(\eta)\,sin(B\xi) + \theta_{3a}(\eta)\,cos(B\xi) \tag{11}$$

$$\varphi_b(\eta,\xi) = \theta_{0b}\left(\frac{1}{Gz} - \xi\right) + \theta_{1b}(\eta) + \theta_{2b}(\eta)\,sin(B\xi) + \theta_{3b}(\eta)\,cos(B\xi) \tag{12}$$

in which the θ_{0a} and θ_{0b} are the constants and the $\theta_{1a}(\eta)$, $\theta_{2a}(\eta)$, $\theta_{3a}(\eta)$, $\theta_{1b}(\eta)$, $\theta_{2b}(\eta)$ and $\theta_{3b}(\eta)$ are the functions of η yet to be determined. Substituting Eqs (11) and (12) into the governing equations, Eqs (1) and (2), and the boundary conditions, Eqs (3)−(6), yields

$$\begin{aligned}&\theta_{0a}\xi + \theta_{1a}(\kappa) + \theta_{2a}(\kappa)\,sin(B\xi) + \theta_{3a}(\kappa)\,cos(B\xi)\\ &= \theta_{0b}\left(\frac{1}{Gz} - \xi\right) + \theta_{1b}(\kappa) + \theta_{2b}(\kappa)\,sin(B\xi) + \theta_{3b}(\kappa)\,cos(B\xi)\end{aligned} \tag{13}$$

We can apply the Frobenius method which enables one to create a power series solution to solve $\theta_{2a}(\eta)$, $\theta_{3a}(\eta)$, $\theta_{2b}(\eta)$ and $\theta_{3b}(\eta)$ by introducing the complex functions $\psi_a(\eta) = \theta_{2a}(\eta) + \theta_{3a}(\eta)i$ and $\psi_b(\eta) = \theta_{2b}(\eta) + \theta_{3b}(\eta)i$ according to the prior mathematical treatment [51] while solving θ_{0a}, $\theta_{1a}(\eta)$, θ_{0b}, and $\theta_{1b}(\eta)$ with double integrations with respect to ξ in the interval [0, $2\pi/B$]. However, the additional equation of the overall energy balance is required to obtain the average outlet dimensionless temperature φ_F as follows:

$$\rho C_p V(T_F - T_i) = \int_0^L q''(z)2\pi R\,dz \tag{14}$$

or

$$\varphi_F = -\frac{1}{Q_b}\int_\kappa^1 v_b 2\pi R^2 \eta \varphi_b(\eta,0)d\eta \tag{15}$$

Meanwhile, the inlet dimensionless temperature $\varphi_a(\eta,0)$ is defined as

$$\varphi_a(\eta,0) = \frac{k(T_a(r,0)-T_i)}{q_0''R} = \frac{1}{Q_a}\int_0^\kappa v_a 2\pi R^2 \eta \varphi_a(\eta,0)d\eta \tag{16}$$

Now, Type A and other external-recycle configurations are demonstrated and explained using the boundary condition and volumetric flow rate, as summarized in Table 1. The heat-transfer coefficient h is determined from $q_w''(z) = \hbar\left(T_j(R,z) - T_i\right)$ and obtained in the dimensionless form as

$$\hbar = \frac{k}{R}\frac{q_w''(\xi)}{q_0''\varphi_j(1,\xi)} = \frac{k}{R}\frac{1 + sin(B\xi)}{\varphi_j(1,\xi)} \tag{17}$$

The local Nusselt number is defined as

$$Nu(\xi) = \frac{\hbar De}{k} \tag{18}$$

and where k is the heat conductivity coefficient of the fluid, De is the equivalent diameter of the conduit, $De = 2R$. Substituting Eq (17) into Eq (18) yields

$$Nu\ (\xi) = \frac{2[1 + sin(B\xi)]}{\varphi_j(1,\xi)} \tag{19}$$

Similarly, the local Nusselt number of single-pass heat exchangers is defined as

$$Nu_0(\xi) = \frac{2[1 + sin(B\xi)]}{\varphi_0(1,\xi)} \tag{20}$$

where the wall temperature distribution, $\varphi_0(1,\xi)$, of single-pass heat exchangers can be determined, according to the reference [51]. Moreover, the average Nusselt numbers of single- and double-pass concentric circular heat exchangers, respectively, were represented by:

$$\overline{Nu} = Gz\int_0^{1/Gz} Nu(\xi)\,d\xi = Gz\int_0^{1/Gz} \frac{2[1 + sin(B\xi)]}{\varphi_j(1,\xi)}\,d\xi, \text{j} = \text{a,b} \tag{21}$$

and

$$\overline{Nu_0} = Gz\int_0^{1/Gz} Nu_0(\xi)\,d\xi = Gz\int_0^{1/Gz} \frac{2[1 + sin(B\xi)]}{\varphi_0(1,\xi)}\,d\xi \tag{22}$$

The heat-transfer efficiency improvement was illustrated by evaluating the percentage increase in the operation under a double-pass device, which is based on single-pass device with the same working dimensions and operating parameters

$$I_{\hbar} = \frac{\overline{Nu} - \overline{Nu_0}}{\overline{Nu_0}}(\%) \tag{23}$$

Table 1. Volumetric flow rates and boundary conditions for flow Types A−D.

Flow type	Inner channel Q_a	Annular channel Q_b	Boundary Condition, $\xi = 0$	Boundary Condition, $\xi = 1/Gz$
A	$V(1+M)$	$V(1+M)$	$\varphi_a(\eta,0) = \frac{M}{(M+1)}\varphi_b(\eta,0)$	$\varphi_{a,L} = \varphi_{b,L}$
B	$V(1+M)$	V	$\varphi_a(\eta,0) = \frac{M}{(M+1)}\varphi_a\left(\eta,\frac{1}{Gz}\right)$	$\varphi_{a,L} = \varphi_{b,L}$
C	V	$V(1+M)$	$\varphi_a(\eta,0) = 0$	$\varphi_{b,L} = \frac{\varphi_{a,L} + M\varphi_{b,0}}{1+M}$
D	$V(1+M)$	MV	$\varphi_a(\eta,0) = \frac{M}{(M+1)}\varphi_b(\eta,0)$	$\varphi_F = \varphi_{a,L} = \varphi_{b,L}$

Type B: External recycling at the outlet

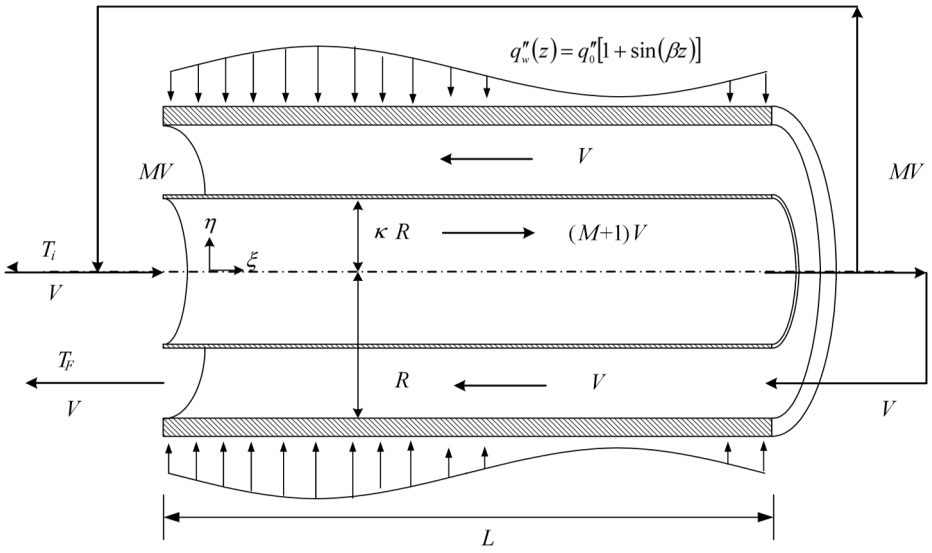

Figure 2. A schematic drawing of recycling double-pass concentric circular heat exchanger (Type B).

Type C: External recycling at the inlet

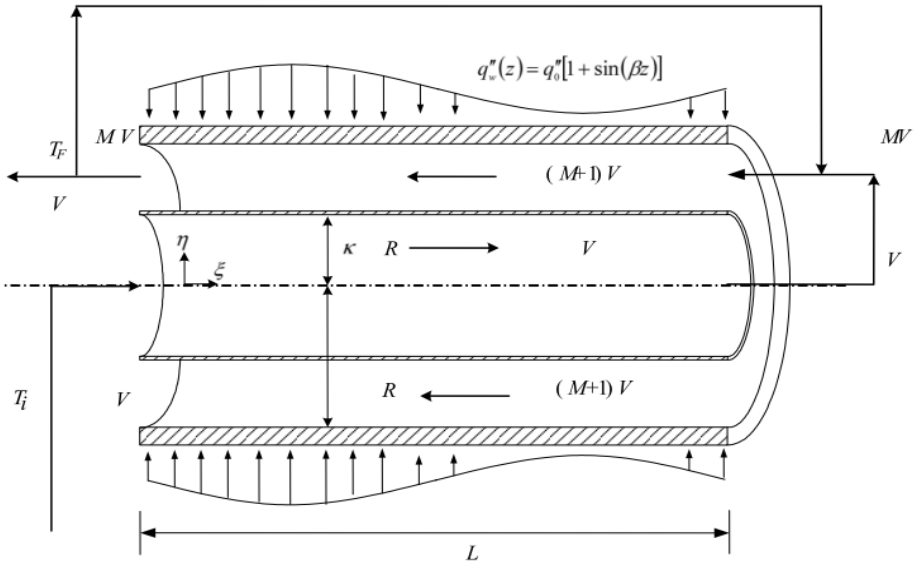

Figure 3. A schematic drawing of recycling double-pass concentric circular heat exchanger (Type C).

Type D: Internal recycling at the outlet

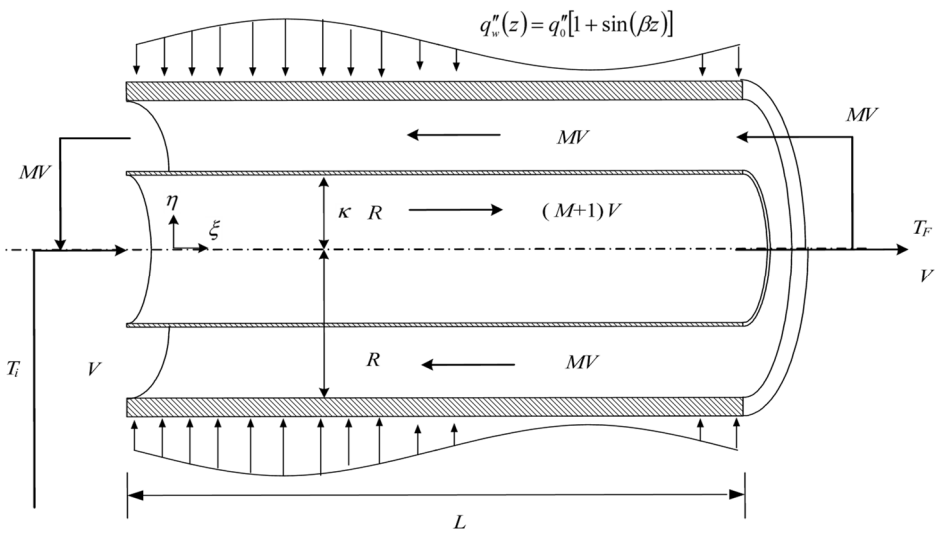

Figure 4. A schematic drawing of recycling double-pass concentric circular heat exchanger (Type D).

3. Results and discussion

The theoretical development of the present study enhances the comprehensive understanding of the heat-transfer behaviors by comparing among double-pass heat exchangers with various external-recycle types, as referred to conjugated Graetz problems. And the wall temperature distributions were determined by solving the mathematical formulations analytically. The mass balance equations of laminar countercurrent-flow double-pass concentric circular heat exchangers with sinusoidal wall fluxes were solved using the linear superposition of Eqs (11) and (12). The dimensionless temperature distributions of power-law fluids in the recycling double-pass device with sinusoidal wall flux can be obtained theoretically by separating the original boundary value problem into a partial differential equation, which can be solved by Frobenius method. The theoretical results of heat-transfer designs enable an engineer to select the appropriate materials and to carefully consider both technical and economic feasibility. The qualitative and quantitative graphs are presented to examine the optimal heat-transfer efficient among various external-recycle types. In this study, the concept of designing the concentric circular double-pass heat exchangers with external recycle is the non-Newtonian fluid to be heated twice in both subchannels before exiting the device. This demonstrates the substantial improvement in the proposed recycling double-pass devices and its heat-transfer efficiency.

It is of critical importance for engineers to evaluate wall temperature distributions beforehand in designing a heat exchanger for cost considerations and practical applicability. The theoretical predictions are demonstrated in Figures 5−7 for various κ values. A larger Graetz number (higher volumetric flow rate) is followed by a shorter residence time of power-law fluids in conduit, which results in the decrease in dimensionless wall temperature and the flatter profiles in all external-recycle configurations. Moreover, the convective heat-transfer coefficient increases with the κ value, and thus, wall temperature oscillations decrease due to a higher average velocity in the annular channel compared to the counterpart in the single-pass operation. The results illustrate the influence

of κ value (impermeable-sheet position) for four flow patterns with external recycle and the dimensionless wall temperature distributions decreasing with κ (relative narrower lumen channel), as shown in Figures 5−7. The temperature of dimensionless wall is lower at the downstream on the outer wall, where the dimensionless wall temperature could reach an extremely low value, particularly for significantly high volumetric flow rate, say Gz = 100. On the contrary, the dimensionless wall temperature of the flow pattern D is the highest one and the magnitude stays at the downstream on the outer wall. The dimensionless wall temperature profiles are monotonically decreasing along the heat-exchanger device toward the end downstream with the same trend for all four external-recycle configurations as well as the single-pass device regardless of the Gz values.

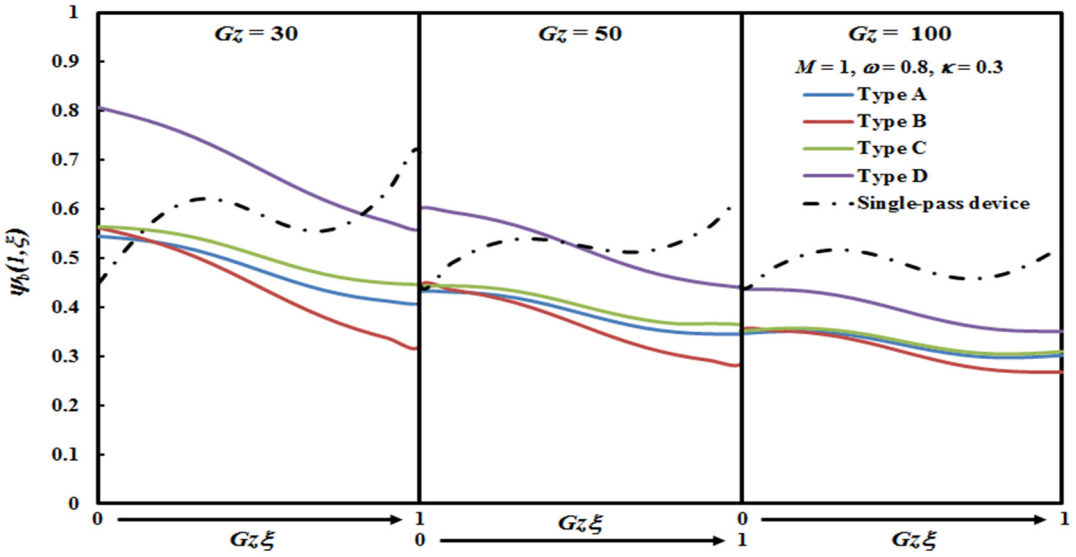

Figure 5. Dimensionless wall temperature distribution with and as parameters with κ = 0.3.

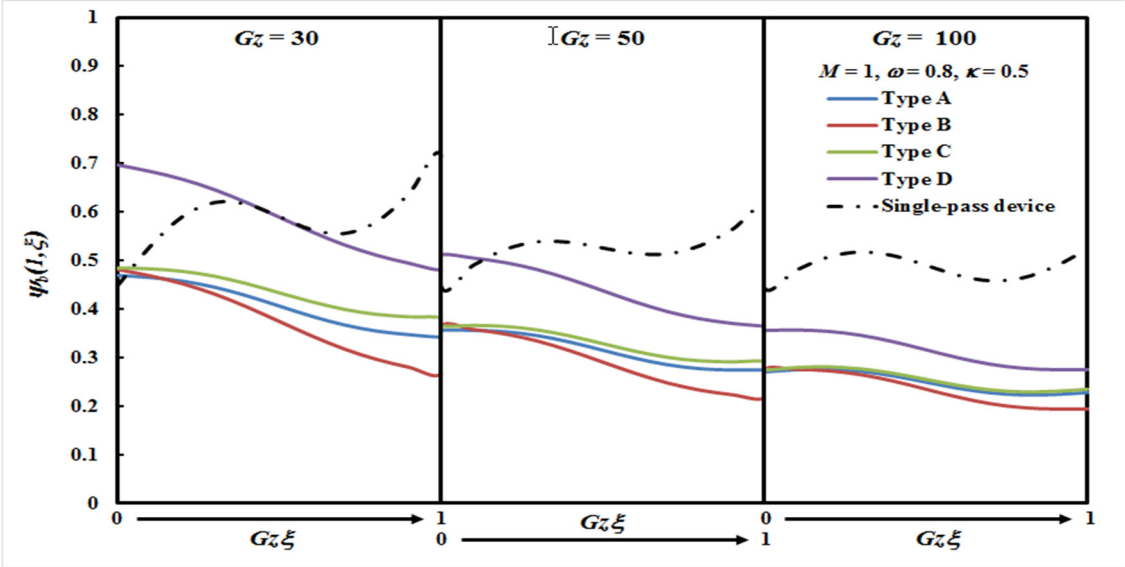

Figure 6. Dimensionless wall temperature distribution with and as parameters with κ = 0.5.

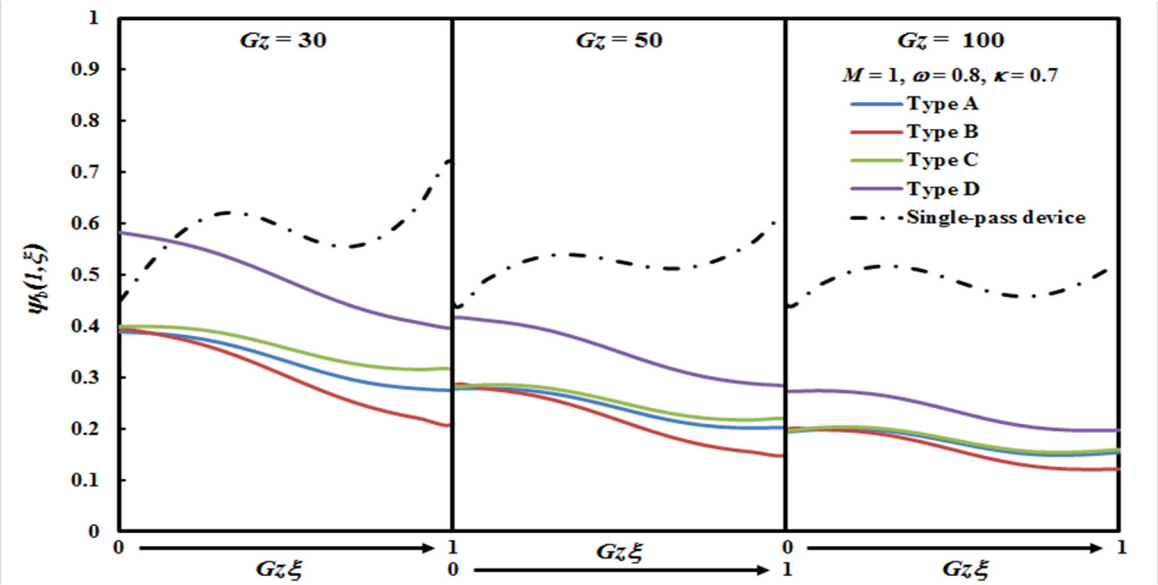

Figure 7. Dimensionless wall temperature distribution with and as parameters with κ = 0.7.

The theoretical predictions of the average Nusselt number and dimensionless outlet temperature developed by this study are listed in Table 2. Similar to the distribution of dimensionless wall temperature, the simulated average Nusselt numbers of four external-recycle types were presented in Figures 8−10 with κ = 0.3, κ = 0.5, and κ = 0.7, respectively. Four flow types of the double-pass concentric circular heat exchanger show the *Nu* number is larger than that in the single-pass device with respect to the heat-transfer efficiency. The device performance also improves with increasing Gz and κ.

Table 2. Theoretical predictions of the average Nusselt numbers and outlet temperature for all types.

Flow type	Average Nusselt numbers	Outlet temperature
A	$\overline{Nu_A} = Gz\int_0^{1/Gz} Nu(\xi)\,d\xi = Gz\int_0^{1/Gz} \frac{2[1+sin(B\xi)]}{\varphi_b(1,\xi)}d\xi$	$\varphi_F = -\frac{1}{(M+1)V}\int_\kappa^1 v_b 2\pi R^2 \eta \varphi_b(\eta,0)d\eta$
B	$\overline{Nu_A} = Gz\int_0^{1/Gz} Nu(\xi)\,d\xi = Gz\int_0^{1/Gz} \frac{2[1+sin(B\xi)]}{\varphi_b(1,\xi)}d\xi$	$\varphi_F = \frac{-1}{V}\int_\kappa^1 v_b 2\pi R^2 \eta \varphi_b(\eta,0)d\eta$
C	$\overline{Nu_A} = Gz\int_0^{1/Gz} Nu(\xi)\,d\xi = Gz\int_0^{1/Gz} \frac{2[1+sin(B\xi)]}{\varphi_b(1,\xi)}d\xi$	$\varphi_F = \frac{-1}{V(M+1)}\int_\kappa^1 v_b 2\pi R^2 \eta \varphi_b(\eta,0)d\eta$
D	$\overline{Nu_A} = Gz\int_0^{1/Gz} Nu(\xi)\,d\xi = Gz\int_0^{1/Gz} \frac{2[1+sin(B\xi)]}{\varphi_b(1,\xi)}d\xi$	$\varphi_F = \frac{1}{V(M+1)}\int_0^\kappa v_a 2\pi R^2 \eta \varphi_a\left(\eta,\frac{1}{Gz}\right)d\eta$

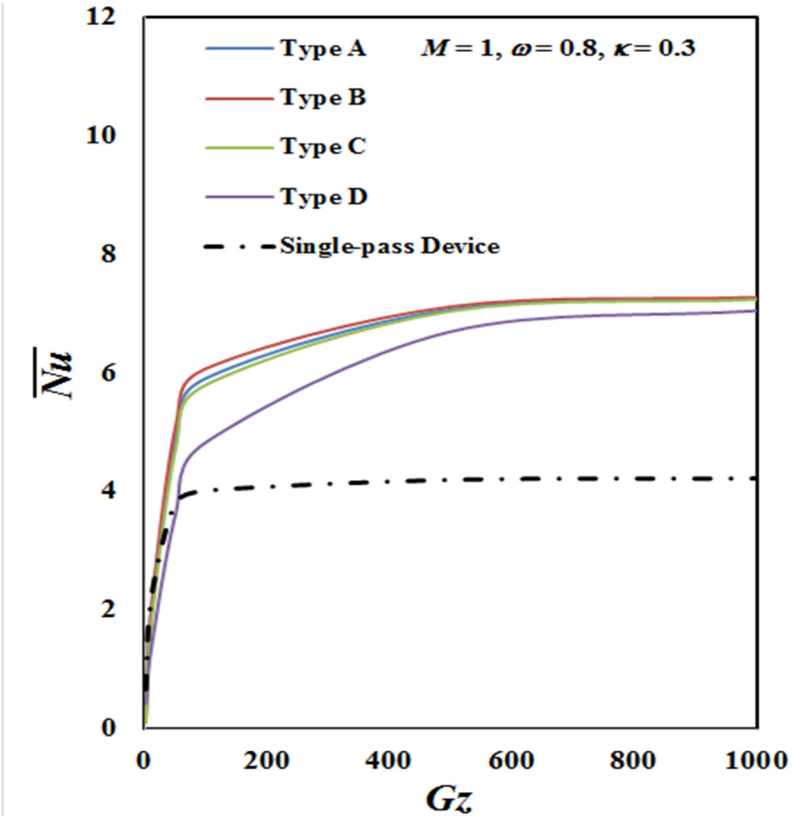

Figure 8. Average Nusselt numbers for four flow patterns and single-pass device with $\kappa = 0.3$.

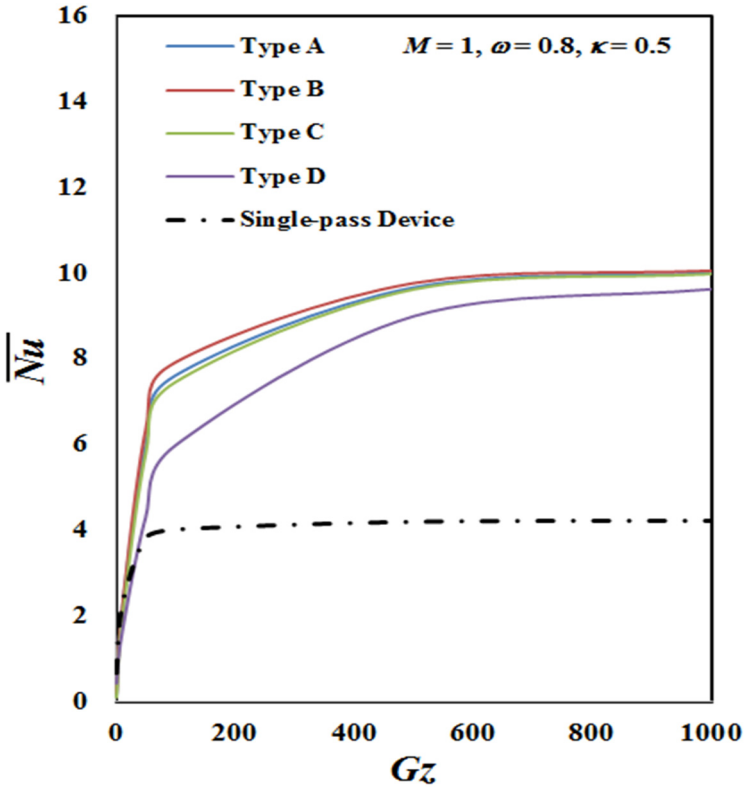

Figure 9. Average Nusselt numbers for four flow patterns and single-pass device with $\kappa = 0.5$.

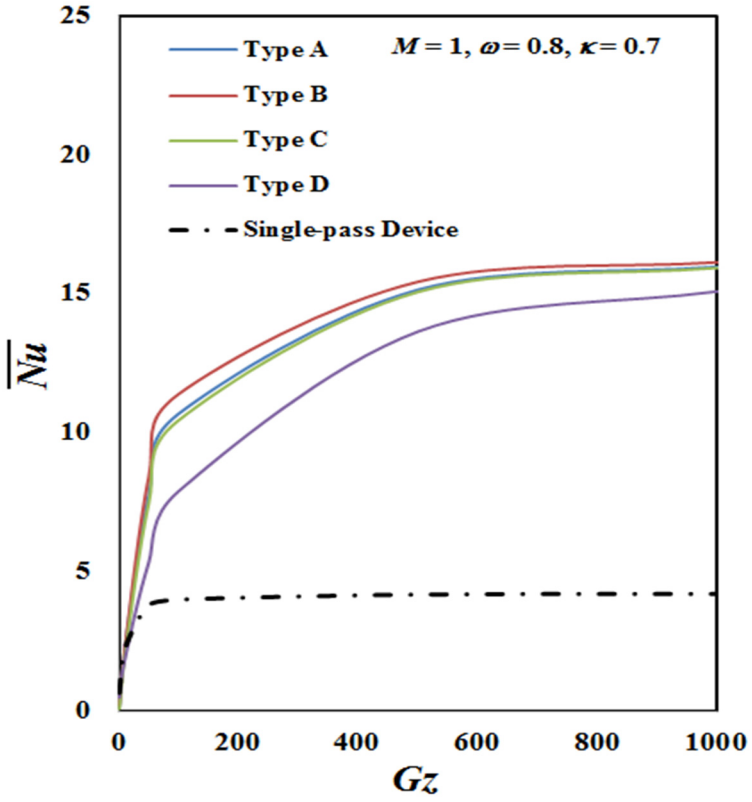

Figure 10. Average Nusselt numbers for four flow patterns and single-pass device with $\kappa = 0.7$.

The comparison of theoretical predictions of Nusselt number *Nu* was conducted for the double-pass heat exchanger with external-recycle operations, as shown by Figures 8−10 to investigate the effect of the channel thickness ratio on heat-transfer efficiency. It is found that the Nusselt number Nu of the present double-pass heat exchanger is sensitive to the values of parameter κ. It indicates that recycling double-pass devices with a lumen channel of less thickness could achieve a higher heat-transfer efficiency. In general, the heat-transfer efficiency augmented by employing the double-pass device with external recycle of Type B is better than those in other external-recycle types. It can also be observed from Figures 8−10 that the order of the Nusselt numbers *Nu* under the setting of double-pass heat exchanger with external-recycle operation goes as the following: Type B > Type A > Type C > Type D. The external-recycle fluid remixing enters into the lumen channel of Type B with a larger amount of the volumetric flow rate of recycle V and exiting outlet temperature T_F. The function of design proves to be more beneficial compared to those of other external-recycle types.

As expected, the increase in volumetric flow rate due to the external recycle could result in greater improvement in heat-transfer efficiency. Meanwhile, employing recycling double-pass configuration for heating power-law fluids (say Type B in the present study) contributes to smaller volumetric flow rate (say V) in annular channel as well as exiting outlet temperature, and thus the heat-transfer efficiency improvement is achieved. Overall, incorporating the external recycle into concentric circular heat exchangers instead of using the circular single-pass device shows a favorable potential to enhance the heat-transfer efficiency in designing the heat exchanger module. A higher κ value indicated that the impermeable sheet was closer to outer wall, the power-law fluid flowed faster in the region adjacent to the wall as compared to the power-law fluid flowing in smaller κ values. Therefore, the power-law

fluids with a larger convective heat-transfer coefficient may transport heat more efficiently from the outer wall under the sinusoidal wall flux, generating a higher Nusselt number, especially for the higher Gz region.

Furthermore, the Fanning friction factor of the recycling double-pass heat exchanger would increase due to inserting an impermeable sheet into a circular single-pass device to conduct double-pass operations. The degree of power consumptions for the single-pass and double-pass operations that only incurs the friction losses to walls is not negligible. It could be obtained by using generalized Bernoulli equation [52] with Fanning friction factor f_F [53]:

$$\ell w_{f,i} = \frac{2f_{F,i}\bar{v}_i^2 L}{De_i}, \qquad i = a, b \tag{21}$$

$$P_{\text{double}} = V\rho\ell w_{f,a} + V\rho\ell w_{f,b}, \quad P_{\text{single}} = V\rho\ell w_{f,0} \tag{22}$$

The relative extents I_P of power consumption increment calculates the percentage increment in the double-pass operation, based on the single-pass device as

$$I_P = \frac{P_{\text{double}} - P_{\text{single}}}{P_{\text{single}}} \times 100\% \tag{23}$$

Operations of recycling concentric circular double-pass heat exchangers include considering heat-transfer efficiency with the average Nusselt number (Eqs 18−20) and the Fanning friction factor (Eqs 21−23), where both heat-transfer efficiency improvement and power consumption increment for all four types of flow behaviors have been calculated. The economic benefit was evaluated by considering the ratio of both heat-transfer improvement enhancement I_h and power consumption increment I_p, say I_h/I_p, which was plotted against Graetz number Gz in Figures 11−13. The power-law fluid was heated twice in operating the double-pass heat exchanger but only once under a single-pass operation. This was because the power-law fluid in the inner channel was heated by the power-law fluid in the annular channel through the impermeable sheet. The heat-transfer efficiency enhancement I_h was calculated with a higher value ($I_h > 0$) for the double-pass device, excluding lower Gz values ($I_h < 0$), where the residence time in the single-pass operating was sufficiently longer than that in operating double-pass configurations. Thus, the ratio of I_h/I_p in Figures 11−13 indicates that the single-pass device is preferred to using double-pass devices.

The energy gain at the expense of the increasing friction loss due to external recycling must be taken into consideration while the power consumption increases due to pumping the non-Newtonian fluid circulation through the two divided subchannels. Thus, a suitable selection was determined by the operating parameters for the recycling double-pass heat exchanger in practical and advantageous applications. The results indicated the convective heat-transfer coefficient enhancement from the recycling concentric circular double-pass heat exchanger could compensate for the power consumption increment under the consideration of the economic feasibility. By comparing the ratio of I_h/I_p to those of recycling double-pass devices with κ and Gz value as parameters, the effects of the external recycle and channel thickness ratio enhance the heat-transfer efficiency in this study, represented by Figures 11−13 for various Graetz number Gz. The ratio of I_h/I_p rapidly increases with Gz and quickly flattens out at a higher Gz number. The power consumption increment of all external-recycle

configurations is not much different from each other except for Type A due to equal volumetric flow rate $(M + 1)V$ in both channels. The trend of power consumption increment for Type A shows no big discrepancy among various κ values, while the profile of Type B and Type C reveals significant variation with the κ value except for Type D (say $\kappa = 0.7$) due to the smaller I_p at a higher κ value. It implies that Type D is better than those of various external-recycle configurations (say Types A, B and C) in improving the heat-transfer efficiency at a higher κ value, as shown in Figure 13.

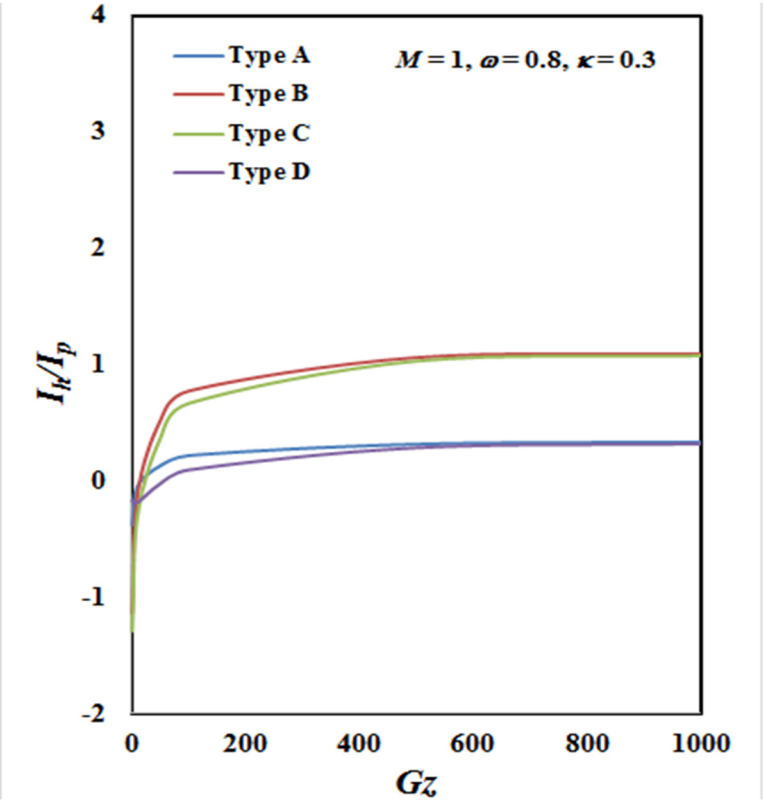

Figure 11. The ratio of I_h/I_p vs. Graetz number Gz.

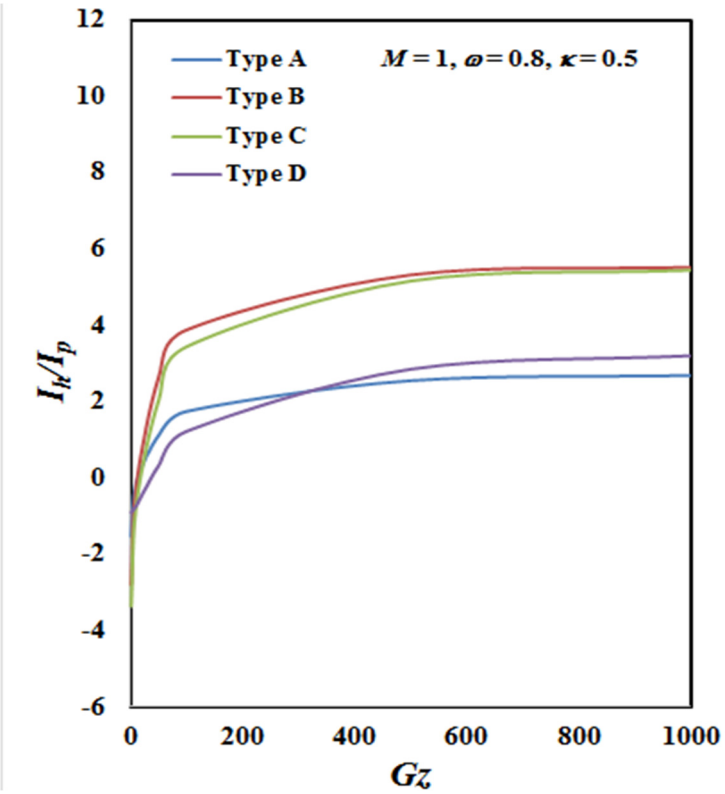

Figure 12. The ratio of I_h/I_p vs. Graetz number Gz.

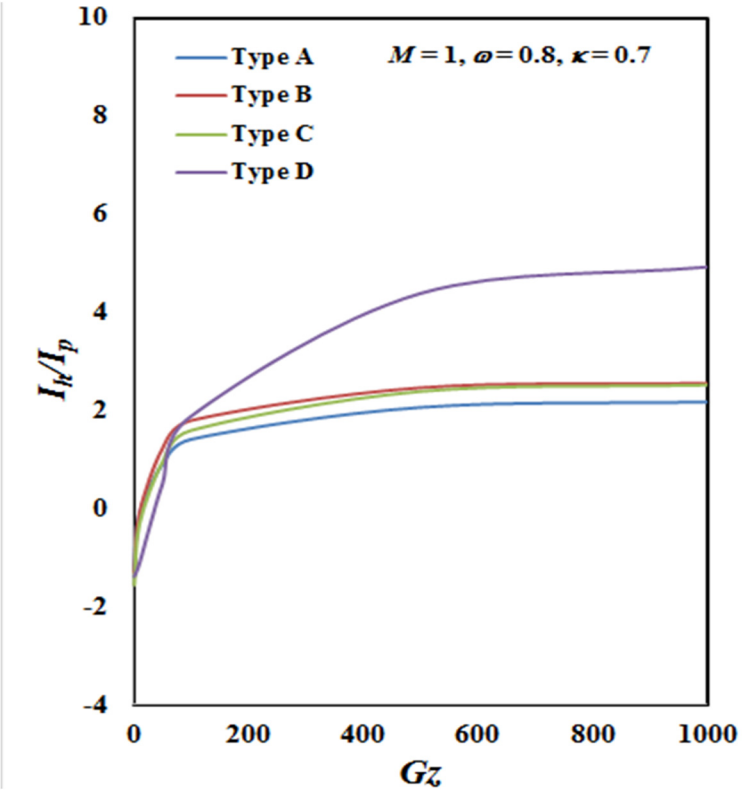

Figure 13. The ratio of I_h/I_p vs. Graetz number Gz.

4. Conclusions

A mathematical formulation for a concentric circular double-pass heat exchanger of power-law fluids with sinusoidal wall flux has been developed under the conjugated Graetz problems. The analytical solution is obtained using a general solution to transform the boundary value problem into a partial differential equation, which can be solved by Frobenius method. Theoretical studies on designing heat-transfer devices of four proposed recycling double-pass configurations are introduced to increase heat-transfer efficiency along with the consideration of the hydraulic dissipated energy increment. Those recycling designs with various thickness ratios and recycle ratios of the channel were operated to enlarge the convective heat-transfer coefficient, which would enhance heat-transfer efficiency compared to the performance under circular single-pass device, as shown in Figures 8−10. By comparing with the circular single-pass device, the present study validates the thermal performance of the various external-recycle configurations of concentric circular double-pass heat exchangers as proposed. These four external-recycle types result in a better device performance due to the augmented convective heat-transfer coefficient and enlarged heat-transfer area coupled with a relatively smaller power consumption increment. Also, the three graphical illustrations, on the ratio of I_h/I_p vs. Graetz number Gz, showcase economic potential of the operation where there is rise in the ratio of the heat-transfer efficiency improvement over power consumption increment, as indicated in Figures 11−13.

In this theoretical study, recycling concentric circular double-pass heat exchangers were examined across four configurations with external recycle under various operational conditions. The conclusive findings are summarized as follow:

1) A simplified mathematical formulation was obtained for double-pass concentric circular heat exchangers to analyze heat transfer problems with sinusoidal wall fluxes at boundaries.

2) The improvement in heat-transfer efficiency of concentric circular double-pass heat exchangers increases with M, Gz and κ.

3) The external-recycle configuration (say Type B in the present study) serves as an important economic advantage in designing concentric circular heat exchangers for the heating of power-law fluids associated with the smaller volumetric flow rate in annular channel with exit outlet temperature.

4) The dimensionless wall temperature distributions decrease as κ increases (relative narrower lumen channel).

5) Under economic consideration, Type D is better than those of various external-recycle configurations (say Types A, B and C) in improving the heat-transfer efficiency at higher κ values, while the single-pass device is preferred to the double-pass devices at lower Gz values.

6) The economic feasibility in designing recycling double-pass devices is demonstrated by the optimal operating condition at higher κ value that reasonably compensates for a relative lower power consumption increment.

Acknowledgments

The authors wish to thank the Ministry of Science and Technology (MOST) of the Republic of China for its financial support.

Conflict of interest

The authors have no conflict of interest.

References

1. R. K. Shah, A. L. London, *Laminar Flow Forced Convection in Ducts*, Academic Press, New York, U.S.A., (1978), 196–207. https://doi.org/10.1016/C2013-0-06152-X
2. V. D. Dang, M. Steinberg, Convective diffusion with homogeneous and heterogeneous reaction in a tube, *J. Phys. Chem.*, **84** (1980), 214−219. https://doi.org/10.1021/j100439a018
3. E. Papoutsakis, D. Ramkrishna, Conjugated Graetz problems. I: General formalism and a class of solid-fluid problems, *Chem. Eng. Sci*., **36** (1981), 1381−1391. https://doi.org/10.1016/0009-2509(81)80172-8
4. X. Yin, H. H. Bau, The Conjugated Greatz problem with axial conduction, *Trans. ASME*, **118** (1996), 482−485. https://doi.org/10.1115/1.2825871
5. D. Kaya, H. I. Sarac, Mathematical modeling of multiple-effect evaporators and energy economy, *Energy*, **32** (2007), 1536−1542. https://doi.org/10.1016/j.energy.2006.09.002
6. J. Li, P. Hrnjak, Separation in condensers as a way to improve efficiency, *Int. J. Refrig.*, **79** (2017), 1−9. https://doi.org/10.1016/j.ijrefrig.2017.03.017
7. F. Reyes, W. L. Luyben, Extensions of the simultaneous design of gas-phase adiabatic tubular reactor systems with gas recycle, *Ind. Eng. Chem. Res.*, **40** (2001), 635−647. https://doi.org/10.1021/ie000603j
8. C. M. C. Bonelli, A. F. Martins, E. B. Mano, C. L. Beatty, Effect of recycled polypropylene on polypropylene/high-density polyethylene blends, *J. Appl. Polym. Sci.*, **80** (2001), 1305−1311. https://doi.org/10.1002/app.1217
9. M. A. Ebadian, H. Y. Zhang, An exact solution of extended Graetz problem with axial heat conduction, *Int. J. Heat Mass Transfer*, **32** (1989), 1709−1717. https://doi.org/10.1016/0017-9310(89)90053-7
10. C. Heinen, G. Guthausen, H. Buggisch, Determination of the power law exponent from magnetic resonance imaging (MRI) flow data, *Chem. Eng. Technol.*, **25** (2002), 873–877. https://doi.org/10.1002/1521-4125(20020910)25:9<873::AID-CEAT873>3.0.CO;2-T
11. R. P. Bharti, R. P. Chhabra, V. Eswaran, Steady forced convection heat transfer from a heated circular cylinder to power-law fluids, *Int. J. Heat Mass Transfer*, **50** (2007), 977−990. https://doi.org/10.1016/j.ijheatmasstransfer.2006.08.008
12. A. Carezzato, M. R. Alcantara, J. Telis-Romero, C. C. Tadini, J. A. W. Gut, Non-Newtonian heat transfer on a plate heat exchanger with generalized configurations, *Chem. Eng. Technol.*, **32** (2007), 21–26. https://doi.org/10.1002/ceat.200600294
13. A. A. Delouei, M. Nazari, M. H. Kayhani, G. Ahmadi, Direct-forcing immersed boundary – non-Newtonian lattice Boltzmann method for transient non-isothermal sedimentation, *J. Aerosol Sci.*, **104** (2017), 106−122. https://doi.org/10.1016/j.jaerosci.2016.09.002
14. A. A. Delouei, M. Nazari, M. H. Kayhani, G. Ahmadi, A non-Newtonian direct numerical study for stationary and moving objects with various shapes: An immersed boundary – Lattice Boltzmann approach, *J. Aerosol Sci.*, **93** (2016), 45−62. https://doi.org/10.1016/j.jaerosci.2015.11.006

15. A. A. Delouei, M. Nazari, M. H. Kayhani, S. Succi, Non-Newtonian unconfined flow and heat transfer over a heated cylinder using the direct-forcing immersed boundary–thermal lattice Boltzmann method, *Phys. Rev. E*, **89** (2014), 053312. https://doi.org/10.1103/PhysRevE.89.053312
16. A. Jalali, A. A. Delouei, M. Khorashadizadeh, A. M. Golmohamadi, S. Karimnejad, Mesoscopic simulation of forced convective heat transfer of Carreau-Yasuda fluid flow over an inclined square: Temperature-dependent viscosity, *J. Appl. Comput. Mech.*, **6** (2020), 307−319. https://doi.org/10.22055/JACM.2019.29503.1605
17. S. Aghakhani, A. H. Pordanjani, A. Karimipour, A. Abdollahi, M. Afrand, Numerical investigation of heat transfer in a power-law non-Newtonian fluid in a C-Shaped cavity with magnetic field effect using finite difference lattice Boltzmann method, *Comput. Fluids*, **176** (2018), 51−67. https://doi.org/10.1016/j.compfluid.2018.09.012
18. J. M. Buick, Lattice Boltzmann simulation of power-law fluid flow in the mixing section of a single-screw extruder, *Chem. Eng. Sci.*, **64** (2009), 52−58. https://doi.org/10.1016/j.ces.2008.09.016
19. C. Y. Xie, J. Y. Zhang, V. Bertola, M. Wang, Lattice Boltzmann modeling for multiphase viscoplastic fluid flow, *J. Non-Newtonian Fluid Mech.*, **234** (2016), 118−128.
20. C. D. Ho, G. G. Lin, W. H. Lan, Analytical and experimental studies of power-law fluids in double-pass heat exchangers for improved device performance under uniform heat fluxes, *Int. J. Heat Mass Transfer*, **61** (2013), 464−474. https://doi.org/10.1016/j.ijheatmasstransfer.2013.02.007
21. S. Karimnejad, A. A. Delouei, M. Nazari, M. Shahmardan, A. Mohamad, Sedimentation of elliptical particles using Immersed Boundary–Lattice Boltzmann Method: A complementary repulsive force model, *J. Mol. Liq.*, **262** (2018), 180−193. https://doi.org/10.1016/j.molliq.2018.04.075
22. S. Karimnejad, A. A. Delouei, M. Nazari, M. Shahmardan, M. Rashidi, S. Wongwises, Immersed boundary-thermal lattice Boltzmann method for the moving simulation of non-isothermal elliptical particles, *J. Therm. Anal. Calorim.*, **138** (2019), 4003−4017. https://doi.org/10.1007/s10973-019-08329-y
23. A. E. F. Monfared, A. Sarrafi, S. Jafari, M. Schaffie, Thermal flux simulations by lattice Boltzmann method; investigation of high Richardson number cross flows over tandem square cylinders, *Int. J. Heat Mass Transfer*, **86** (2015), 563−580. https://doi.org/10.1016/j.ijheatmasstransfer.2015.03.011
24. A. De Rosis, Harmonic oscillations of laminae in non-Newtonian fluids: a lattice Boltzmann-immersed boundary approach, *Adv. Water Resour.*, **73** (2014), 97−107. https://doi.org/10.1016/j.advwatres.2014.07.004
25. E. Aharonov, D. H. Rothman, Non-Newtonian flow (through porous media): A lattice-Boltzmann method, *Geophys. Res. Lett.*, **20** (1993), 679−682. https://doi.org/10.1029/93GL00473
26. A. Amiri Delouei, M. Nazari, M. Kayhani, S. Kang, S. Succi, Non-Newtonian particulate flow simulation: Adirect-forcing immersed boundary–lattice Boltzmann approach, *Physica A*, **447** (2016), 1−20. https://doi.org/10.1016/j.physa.2015.11.032
27. C. J. Ho, W. C. Chen, W. M. Yan, M. Amani, Cooling performance of MEPCM suspensions for heat dissipation intensification in a minichannel heat sink, *Int. J. Heat Mass Transfer*, **115** (2017) 43−49. https://doi.org/10.1016/j.ijheatmasstransfer.2017.08.019

28. C. J. Ho, P. C. Chang, W. M. Yan, P. Amani, Efficacy of divergent minichannels on cooling performance of heat sinks with water-based MEPCM suspensions, *Int. J. Therm. Sci.*, **130** (2018) 333−346. https://doi.org/10.1016/j.ijthermalsci.2018.04.035
29. H. L. Tbena, M. I. Hasan, Numerical investigation of microchannel heat sink with MEPCM suspension with different types of PCM, *Al-Qadisiyah J. Eng. Sci.*, **11** (2018), 115−133. https://doi.org/10.30772/qjes.v11i1.524
30. A. Sarı, C. Alkan, C. Bilgin, A. Bicer, Preparation, characterization and thermal energy storage properties of micro/nano encapsulated phase change material with acrylic-based polymer, *Polym. Sci., Ser. B*, **60** (2018), 58−68. https://doi.org/10.1134/S1560090418010128
31. E. Alehosseini, S.M. Jafari, Micro/nano-encapsulated phase change materials (PCMs) as emerging materials for the food industry, *Trends Food Sci. Technol.*, **91** (2019), 116−128. https://doi.org/10.1016/j.tifs.2019.07.003
32. M. Ghalambaz, J. Zhang, Conjugate solid-liquid phase change heat transfer in heatsink filled with phase change material-metal foam, *Int. J. Heat Mass Transfer*, **146** (2020), 118832−118849. https://doi.org/10.1016/j.ijheatmasstransfer.2019.118832
33. M. Ghalambaz, S. M. H. Zadeh, S. A. M. Mehryan, I. Pop, D. S. Wen, Analysis of melting behavior of PCMs in a cavity subject to a non-uniform magnetic field using a moving grid technique, *Appl. Math. Model.*, **77** (2020), 1936−1953. https://doi.org/10.1016/j.apm.2019.09.015
34. C. J. Ho, Y. C. Liu, M. Ghalambaz, W. M. Yan, Forced convection heat transfer of nano-encapsulated phase change material (NEPCM) suspension in a mini-channel heat sink, *Int. J. Heat Mass Transfer*, **155** (2020), 119858−119870. https://doi.org/10.1016/j.ijheatmasstransfer.2020.119858
35. S. A. M. Mehryan, L. S. Gargari, A. Hajjar, M. Sheremet, Natural convection flow of a suspension containing nano-encapsulated phase change particles in an eccentric annulus, *J. Energy Storage*, **28** (2020), 101236−101273. https://doi.org/10.1016/j.est.2020.101236
36. J. F. Xie, B.Y. Cao, S. A. M. Mehryan, L. S. Gargari, A. Hajjar, M. Sheremet, Natural convection of power-law fluids under wall vibrations: A lattice Boltzmann study, *Numer. Heat Transfer, Part A*, **72** (2017), 600−627. https://doi.org/10.1080/10407782.2017.1394134
37. A. Petrovic, D. Lelea, I. Laza, The comparative analysis on using the NEPCM ma- terials and nanofluids for microchannel cooling solutions, *Int. Commun. Heat Mass Transfer*, **79** (2016), 39−45. https://doi.org/10.1016/j.icheatmasstransfer.2016.10.007
38. A. Hajjar, S. Mehryan, M. Ghalambaz, Time periodic natural convection heat transfer in a nano-encapsulated phase-change suspension, *Int. J. Mech. Sci.*, **166** (2020) 105243. https://doi.org/10.1016/j.ijmecsci.2019.105243
39. M. Ghalambaz, T. Grosan, I. Pop, Mixed convection boundary layer flow and heat transfer over a vertical plate embedded in a porous medium filled with a suspension of nano-encapsulated phase change materials, *J. Mol. Liq.*, **293** (2019), 111432. https://doi.org/10.1016/j.molliq.2019.111432
40. V. D. Zimparov, A. K. da Silva, A. Bejan, Thermodynamic optimization of tree shaped flow geometries with constant channel wall temperature, *Int. J. Heat Mass Transfer*, **49** (2006), 4839−4849. https://doi.org/10.1016/j.ijheatmasstransfer.2006.05.024
41. B. Weigand, D. Lauffer, The extended Graetz problem with piecewise constant wall temperature for pipe and channel flows, *Int. J. Heat Mass Transfer*, **47** (2004), 5303−5312. https://doi.org/10.1016/j.ijheatmasstransfer.2004.06.027

42. A. Behzadmehr, N. Galanis, A. Laneville, Low Reynolds number mixed convection in vertical tubes with uniform wall heat flux, *Int. J. Heat Mass Transfer*, **46** (2003), 4823−4833. https://doi.org/10.1016/S0017-9310(03)00323-5
43. O. Manca, S. Nardini, Experimental investigation on natural convection in horizontal channels with the upper wall at uniform heat flux, *Int. J. Heat Mass Transfer*, **50** (2007), 1075−1086. https://doi.org/10.1016/j.ijheatmasstransfer.2006.07.038
44. C. J. Hsu, Heat transfer in a round tube with sinusoidal wall heat flux distribution, *AIChE J.*, **11** (1965), 690−695. https://doi.org/10.1002/aic.690110423
45. A. Barletta, E. Rossi di Schio, Effects of viscous dissipation on laminar forced convection with axially periodic wall heat flux, *Heat Mass Transfer*, **35** (1999), 9−16. https://doi.org/10.1007/s002310050292
46. D. K. Choi, D. H. Choi, Developing mixed convection flow in a horizontal tube under circumferentially non-uniform heating, *Int. J. Heat Mass Transfer*, **45** (1994), 1899−1913. https://doi.org/10.1016/0017-9310(94)90330-1
47. C. D. Ho, G. G. Lin, T. L. Chew, L. P. Lin, Conjugated heat transfer of power-law fluids in double-pass concentric circular heat exchangers with sinusoidal wall fluxes, *Math. Biosci. Eng.*, **18** (2021), 5592−5613. https://doi.org/10.3934/mbe.2021282
48. R. W. Hanks, K. M. Larsen, The flow of power-law non-Newtonian fluids in concentric annuli, *Ind. Eng. Chem. Fundam.*, **18** (1979), 33−35. https://doi.org/10.1021/i160069a008
49. D. Murkerjee, E. J. Davis, Direct-contact heat transfer immiscible fluid layers in laminar flow, *AIChE J.*, **18** (1972), 94–101. https://doi.org/10.1002/aic.690180118
50. E. J. Davis, S. Venkatesh, The solution of conjugated multiphase heat and mass transfer problems, *Chem. Eng. J.*, **34** (1979), 775–787. https://doi.org/10.1016/0009-2509(79)85133-7
51. A. Barletta, E. Zanchini, Laminar forced convection with sinusoidal wall heat flux distribution: axially periodic regime, *Heat Mass Transfer*, **31** (1995), 41−48. https://doi.org/10.1007/BF02537420
52. J. O. Wilkes, Fluid mechanics for chemical engineers, Prentice-Hall PTR, New Jersey, USA, 1999.
53. J. R. Welty, C. E. Wicks, R. E. Wilson, *Fundamentals of Momentum, Heat, and Mass Transfer*, John Wiley & Sons, New York, USA, 1984.

Appendix

Nomenclature		
De	[m]	hydraulic diameter
f_F	[-]	Fanning friction factor
g_c	[-]	gravity factor
G	[-]	constant
Gz	[-]	Graetz number
H	[-]	constant
h	[kW/mK]	heat transfer coefficient

Continued on next page

Nomenclature		
I_h	[-]	heat-transfer improvement enhancement
I_p	[-]	power consumption increment
k	[kW/mK]	thermal conductivity of the fluid
L	[m]	conduit length
ℓw_f	[kJ/kg]	friction loss in conduit
$\overline{Nu}$	[-]	the average Nusselt number
P	[(Nm)/s]	power consumption
q''	[kW]	wall heat flux
r	[m]	radius coordinate
R	[m]	outer tube radius
R_1	[m]	inter tube radius
T	[K]	temperature of fluid in conduit
V	[m^3/s]	inlet volumetric flow rate
v	[m/s]	velocity distribution of fluid
z	[m]	longitudinal coordinate
α	[m^2/s]	thermal diffusivity of fluid
β	[1/m]	constant
$\dot{\gamma}$	[1/s]	shear rate
δ	[m]	impermeable sheet thickness
ϵ	[-]	coefficients
η	[-]	dimensionless radius coordinate, = *r/R*
κ	[-]	channel thickness ratio
λ	[-]	constant
ξ	[-]	dimensionless longitudinal coordinate = *z/LGz*
ρ	[kg/m^3]	density of the fluid
τ	[Pa]	shear stress
φ	[-]	dimensionless temperature $k(T-T_i)/q_0''R$
ω	[-]	power-law index
ψ	[-]	complex functions of dimensionless temperature

Subscripts		
0	[-]	= at the inlet or for the single-pass device
a	[-]	= the inner flow channel
b	[-]	= the outer flow channel
F	[-]	= at the outlet of a double-pass device
i	[-]	= at the inlet of a double-pass device
L	[-]	= at the end of the channel
w	[-]	= at the wall surface

AIMS Press